

Interference between two resonant transitions with distinct initial and final states connected by radiative decay

A. Marsman, M. Horbatsch and E.A. Hessels*

Department of Physics and Astronomy, York University, Toronto, Ontario M3J 1P3, Canada

(Dated: March 13, 2022)

The resonant line shape from driving a transition between two states, $|a\rangle$ and $|b\rangle$, can be distorted due to a quantum-mechanical interference effect involving a resonance between two different states, $|c\rangle$ and $|d\rangle$, if $|c\rangle$ has a decay path to $|a\rangle$ and $|d\rangle$ has a decay path to $|b\rangle$. This interference can cause a shift of the measured resonance, despite the fact that the two resonances do not have a common initial or final state. As an example, we demonstrate that such a shift affects measurements of the atomic hydrogen $2S_{1/2}$ -to- $2P_{1/2}$ Lamb-shift transition due to $3S$ -to- $3P$ transitions if the $3S_{1/2}$ state has some initial population.

PACS numbers: \pacs{32.70.Jz, 06.20.Jr}

I. INTRODUCTION

Recently, the effect of quantum-mechanical interference on precision measurements has been investigated by the present authors [1–6] and by others [7–16]. These investigations indicate that interference with a neighboring resonance, even if it is very distant, can lead to significant shifts for precision measurements. All of the investigations involve the interference between a pair of resonances that have a common initial state. Here we investigate the interference between two resonances that do not have a common initial state, nor a common final state. We find that an interference between two such resonances exists if the four states are connected by radiative decay, and this interference causes a shift of the measured resonance center.

We explore the implications of this type of effect on the precision measurement of the atomic hydrogen $2S_{1/2}$ -to- $2P_{1/2}$ Lamb shift, which was measured by Lundeen and Pipkin [17] some time ago, and is currently being remeasured by our group. We find that a shift in this measured resonance can be present if there is an initial population in the $3S_{1/2}$ state, due to interference between the $2S_{1/2}$ -to- $2P_{1/2}$ resonance and the $3S_{1/2}$ -to- $3P$ resonances. The hydrogen Lamb-shift measurement has become important since it can, when compared to very precise theory [18], determine the charge radius of the proton. More precise determinations of this radius have now been performed using muonic hydrogen [19, 20], but there is a large discrepancy between measurements made using ordinary hydrogen and muonic hydrogen. This discrepancy has become known as the proton size puzzle [21–23].

II. FOUR-LEVEL SYSTEM

We first consider a four-level system consisting of states $|a\rangle$, $|b\rangle$, $|c\rangle$, and $|d\rangle$, as shown in Fig. 1. An electric

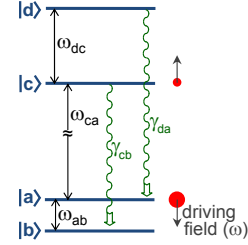


FIG. 1. (Color online) Energy-level diagram for a four-level system. States $|c\rangle$ and $|d\rangle$ radiatively decay to $|b\rangle$ and $|a\rangle$, respectively. When driving the $|a\rangle$ -to- $|b\rangle$ transition, any population in $|c\rangle$ can be driven (by far-off-resonance radiation) to $|d\rangle$. An interference between the $|a\rangle$ -to- $|b\rangle$ and $|c\rangle$ -to- $|d\rangle$ transitions, as described in the text, leads to a distortion of the line shape, and a shift of the $|a\rangle$ -to- $|b\rangle$ resonance line center.

field $\vec{E}(t) = E_0 \hat{z} \cos(\omega t + \phi)$ drives the $|a\rangle$ -to- $|b\rangle$ electric-dipole transition, depleting the initially populated $|a\rangle$ state. The two other states, $|c\rangle$, and $|d\rangle$, are also assumed to be connected by an electric-dipole matrix element, but the transition between these two states is far out of resonance with $\vec{E}(t)$. Since $|d\rangle$ decays radiatively to $|a\rangle$, any initial population in $|c\rangle$ that is weakly driven by the off-resonant field to $|d\rangle$ slightly enhances the population of the $|a\rangle$ state. A more efficient method of transferring population from $|c\rangle$ to $|a\rangle$ involves an interference between the on-resonant $|a\rangle$ -to- $|b\rangle$ transition amplitude and the off-resonant $|c\rangle$ -to- $|d\rangle$ transition, which is possible because of the radiative decay from a coherence between $|c\rangle$ and $|d\rangle$ to a coherence between $|a\rangle$ and $|b\rangle$. The relevant equations for the density matrix for the four-level system are

$$\dot{\rho}_{aa} = iV_{ab}^* \rho_{ab} - iV_{ab} \rho_{ba} + \gamma_{da} \rho_{dd}, \quad (1a)$$

$$\dot{\rho}_{bb} = iV_{ab} \rho_{ba} - iV_{ab}^* \rho_{ab} + \gamma_{cb} \rho_{cc}, \quad (1b)$$

$$\dot{\rho}_{ba} = i\omega_{ab} \rho_{ba} + iV_{ab}^* (\rho_{bb} - \rho_{aa}) \pm \sqrt{\gamma_{da} \gamma_{cb}} \rho_{cd}, \quad (1c)$$

$$\dot{\rho}_{cc} = iV_{cd}^* \rho_{cd} - iV_{cd} \rho_{dc} - \gamma_{cb} \rho_{cc}, \quad (1d)$$

$$\dot{\rho}_{dd} = iV_{cd} \rho_{dc} - iV_{cd}^* \rho_{cd} - \gamma_{da} \rho_{dd}, \quad (1e)$$

$$\dot{\rho}_{cd} = i\omega_{cd} \rho_{cd} + iV_{cd} (\rho_{cc} - \rho_{dd}) - \frac{\gamma_{da} + \gamma_{cb}}{2} \rho_{cd}, \quad (1f)$$

* hessels@yorku.ca

where $V_{ij}(t) = \langle i | e\vec{E}(t) \cdot \vec{r} | j \rangle / \hbar$, and Fig. 1 shows the energy separations, $\hbar\omega_{ij}$, and decay rates, γ_{ij} . Of particular interest in these equations is the square-root term, which allows for the coherence between $|c\rangle$ and $|d\rangle$ to be transferred via radiative decay to a coherence between $|a\rangle$ and $|b\rangle$. This term [24] is often incorrectly omitted in the treatment of density matrices. The sign of the term depends on the relative sign of the a-to-d and b-to-c matrix elements that are responsible for the radiative decay.

Figure 2 shows the results of integrating Eq. (1) from $t=0$ to $t=t_f$ for one choice of the parameters of Eq. (1), with an initial population in $|a\rangle$ ($\rho_{aa}(0)=1$, Fig. 2(a)) and with an initial population in $|c\rangle$ ($\rho_{cc}(0)=1$, Fig. 2(b) and (c)). The line shapes are averaged over the phase ϕ of the driving field. An initial population in $|a\rangle$ leads to a simple resonance at $f = \frac{\omega_{ab}}{2\pi}$, as shown in Fig. 2(a). For the small value of E_0 used, it is well approximated by the perturbative expression

$$\rho_{aa}(t_f) = 1 - \frac{V_{ab}^2 \sin^2(\Delta\omega t_f/2)}{\Delta\omega^2}, \quad (2)$$

where $\Delta\omega = \omega - \omega_{ab}$.

An examination of Eq. (1) reveals that the three lowest-order routes for an initial population in $|c\rangle$ to get to state $|a\rangle$ are

$$\rho_{cc} \rightarrow \rho_{cd}, \rho_{dc} \rightarrow \rho_{dd} \rightarrow \rho_{aa}, \quad (3a)$$

$$\rho_{cc} \rightarrow \rho_{bb} \rightarrow \rho_{ba}, \rho_{ab} \rightarrow \rho_{aa}, \quad (3b)$$

$$\text{and } \rho_{cc} \rightarrow \rho_{cd}, \rho_{dc} \rightarrow \rho_{ba}, \rho_{ab} \rightarrow \rho_{aa}. \quad (3c)$$

Eq. (3a) leads to a resonance centered at $f = \frac{\omega_{dc}}{2\pi}$, and such a resonance is clearly seen in Fig. 2(b). When the scale is expanded by a factor of 100 (dashed line in Fig. 2(b)), the smaller resonance at $f = \frac{\omega_{ab}}{2\pi}$ caused by Eq. (3b) is visible.

The result shown in Fig. 2(b) is calculated by artificially suppressing the square-root term in Eq. (1c). The additional effect of this term is shown in Fig. 2(c), with the solid curve showing the result for the positive sign of this term and the dashed curve for the negative sign. These curves show the effect due to Eq. (3c). For the small values of the V and γ parameters used for Fig. 2, the effect of the square-root term can be approximated by the perturbative expression

$$\Delta\rho_{aa}(t_f) = \frac{\pm\sqrt{\gamma_{cb}\gamma_{da}} t_f V_{ab}V_{cd}}{2\Delta\omega(\omega_{dc} - \omega_{ab})} \left(1 - \frac{\sin(\Delta\omega t_f)}{\Delta\omega t_f}\right). \quad (4)$$

A comparison (for the positive choice of sign) of this perturbative expression to the full result of Fig. 2(c) is shown in Fig. 2(d).

Figure 2 shows that the measurement of the line center of the $|a\rangle$ -to- $|b\rangle$ resonance can be affected by a population in $|c\rangle$. A small distortion and shift of the $|a\rangle$ -to- $|b\rangle$ resonance results from the long tail of the resonance at $\frac{\omega_{dc}}{2\pi}$ (as seen by the dashed line in Fig. 2(b)), which leads to a sloped background under the $|a\rangle$ -to- $|b\rangle$ resonance of

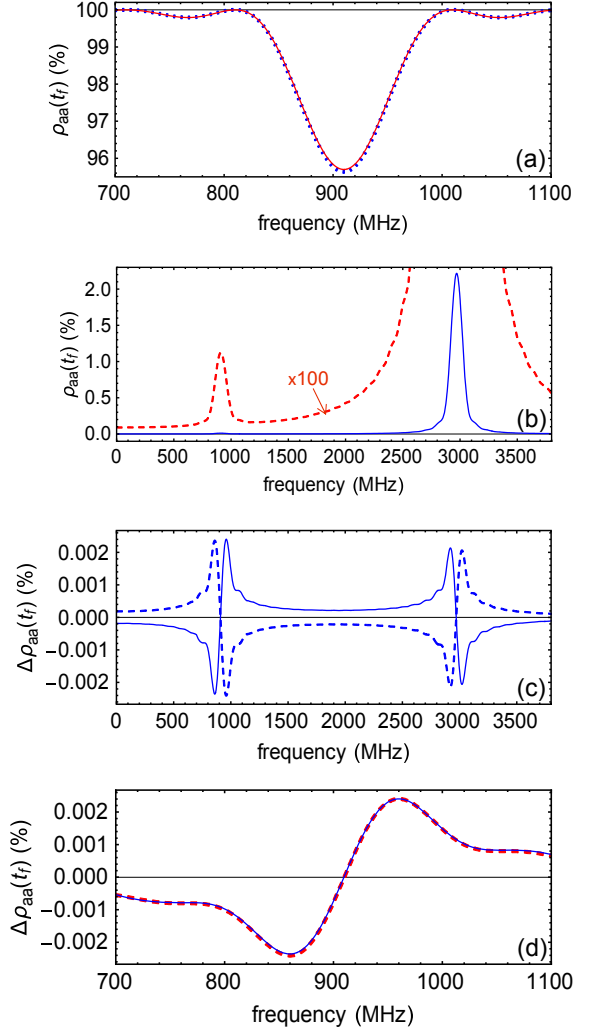


FIG. 2. (Color online) Line shapes for a four-level system with initial population in $|a\rangle$ (a), and for initial population in $|c\rangle$ (b, c, and d). The solid, red line in (a) is the full calculation, with the dotted, blue line showing the perturbative approximation of Eq. (2). The larger resonance in (b) is from driving the $|c\rangle$ -to- $|d\rangle$ transition, followed by decay down to $|a\rangle$. The smaller resonance (expanded by a factor of 100 in the dashed curve) results from radiative decay to $|b\rangle$, followed by driving of the $|b\rangle$ -to- $|a\rangle$ transition. The line shape in (b) artificially suppresses the effect of the coherent decay term (the square-root term in Eq. (1c)). The effect of this term is shown in (c), with the solid and dashed lines showing the effects for the positive and negative signs of the term. This distortion, for the positive case, is shown on a larger scale in (d), along with the perturbative approximation of Eq. (4). When measuring the line center of the resonance in (a), a population in state $|c\rangle$ can cause a shift in this resonance due to the dispersion line shape of (c). For these plots, the parameters used (See Eq. (1) and Fig. 1) are: $\omega_{ba}=2\pi(909.874 \text{ MHz})$, $\omega_{dc}=2\pi(2970.292 \text{ MHz})$, $\gamma_{da}=14.949 \text{ MHz}$, $\gamma_{cb}=0.701 \text{ MHz}$, $V_{ab}=13.925 \frac{\text{MHz}}{\sqrt{\text{cm}}} E(t)$, $V_{cd}=-48.238 \frac{\text{MHz}}{\sqrt{\text{cm}}} E(t)$, $t_f=10 \text{ ns}$, and $E_0=3 \text{ V/cm}$.

Fig. 2(a). If $|a\rangle$ and $|c\rangle$ start with equal populations, the effect of this slope is to shift the $|a\rangle$ -to- $|b\rangle$ resonance by only 0.4 kHz for the parameters used in the figure.

A larger shift results from the effect of Eq. (3c) (Fig. 2(c) and (d)). The dispersion line shape due to this interference effect, causes a shift of 33 kHz for the parameters used in Fig. 2. This shift is independent of E_0 for small values of E_0 , since Fig. 2(a) and Fig. 2(c) both scale as E_0^2 below saturation, as can be seen from Eqs. (2) and (4). Examination of these equations at $\Delta\omega = \pm\pi/t_f$ (points near half maximum) shows that the shift due to the effect of the interference can be approximated by

$$\Delta f = \mp \frac{\pi}{8} \frac{1}{t_f} \frac{V_{cd}}{V_{ab}} \frac{\sqrt{\gamma_{cb}\gamma_{da}}}{(\omega_{dc} - \omega_{ab})} \frac{\rho_{cc}(t=0)}{\rho_{aa}(t=0)}. \quad (5)$$

The result is a shift that persists, even when extrapolated to zero intensity for the driving field. For higher E_0 , the shift becomes somewhat larger since the resonance being measured saturates, while the distortion of Fig. 2(c) continues to increase.

III. SEPARATED OSCILLATORY FIELDS

Shifts are also found when the method of separated oscillatory fields (SOF) [25] is used for the measurement. For SOF measurements, a field of amplitude E_0 and phase ϕ is present from $t=0$ to $t=t_D$, and a second field of the same amplitude that is either in phase or out of phase by 180 degrees (ϕ or $\phi + \pi$) is present from $t=t_S$ to $t=t_S + t_D$. The SOF line shape is the difference between the in-phase and out-of-phase signals.

Integrating Eq. (1) from $t=0$ to $t=t_f=t_D + t_S$ for the SOF fields for one choice of the parameters leads to the line shapes of Fig. 3. For an initial population in $|a\rangle$, Fig. 3(a) shows that the final population exhibits a typical SOF line shape. This line shape is well approximated by its perturbative expression

$$\frac{-4V_{ab}^2 \sin^2(\Delta\omega t_D/2)}{\Delta\omega^2} \cos(\Delta\omega t_S), \quad (6)$$

as shown by the dotted line.

The line shape is distorted if there is any starting population in $|c\rangle$. The large feature centered at $\omega = \omega_{dc}$ in Fig. 3(b) is due to Eq. (3a), and the much smaller feature centered at $\omega = \omega_{ab}$ results from Eq. (3b). The more important feature is due to Eq. (3c), and this interference feature is shown separately in Fig. 3(c), for both the positive (solid) and negative (dashed) choices of sign in Eq. (1c). The perturbative expression

$$\mp 4\sqrt{\gamma_{cb}\gamma_{da}} V_{ab} V_{cd} \frac{\sin^2(\Delta\omega t_D/2)}{\Delta\omega^2(\omega_{dc} - \omega_{ab})} \sin(\Delta\omega t_S), \quad (7)$$

is a good approximation for the distortion for small E_0 , as shown by the dotted red line in Fig. 3(c).

The shifts caused by population in $|c\rangle$ can be estimated using the central zero-crossing positions in Fig. 3(a).

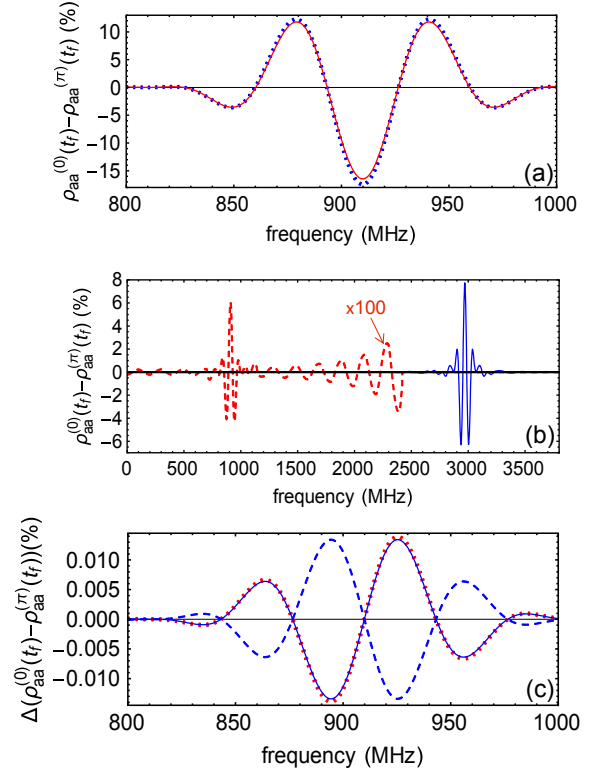


FIG. 3. (Color online) Line shapes for a four-level system using separated oscillatory fields. Initial population in $|a\rangle$ leads to a typical SOF line shape, (a), that is well approximated by a perturbative expression (dotted line). Initial population in $|c\rangle$ (b and c) leads to features due to the $|c\rangle$ -to- $|d\rangle$ transition (the large feature in (b)), due to the $|b\rangle$ -to- $|a\rangle$ transition (the smaller feature in (b), expanded by a factor of 100 in the dashed curve), and an interference between these two resonances, as shown in (c) with both the positive (solid blue line) and negative (dashed blue line) sign choices in Eq. (1c). The perturbative approximation (Eq. (7)) for the positive sign is shown by the dotted red line. When measuring the line center of the resonance in (a), a population in state $|c\rangle$ can cause a shift in this resonance due to the dispersion line shape of (c). For these plots, the parameters used are as in Fig. 2, with $t_D=10$ ns, and $t_S=15$ ns.

Using this method, the effects of Eq. (3a) and (3b) (Fig. 3(b)) lead to a shift of +1.3 kHz for the parameters used in the figure, and the effect of the interfering term, Eq. (3c) (Fig. 3(c)), leads to a shift of ∓ 9.3 kHz. From an examination of Eqs. (6) and (7), it can be seen that this shift is given by

$$\Delta f = \mp \frac{1}{\pi} \frac{1}{2t_S} \frac{V_{cd}}{V_{ab}} \frac{\sqrt{\gamma_{cb}\gamma_{da}}}{(\omega_{dc} - \omega_{ab})} \frac{\rho_{cc}(t=0)}{\rho_{aa}(t=0)}. \quad (8)$$

As in Section II, for small E_0 , the shifts are independent of field strength, and therefore the shifts persist even in the limit of zero field. Both Eq. (5) and Eq. (8) show that the scale of the shift is

$$\frac{V_{cd}}{V_{ab}} \frac{\sqrt{\gamma_{cb}\gamma_{da}}}{(\omega_{dc} - \omega_{ab})} \frac{\rho_{cc}(t=0)}{\rho_{aa}(t=0)} \quad (9)$$

times the width of the resonance.

IV. THE $H(n=2)$ LAMB SHIFT

The interference effects described in the previous sections will affect a precision measurement of the $n=2$ Lamb shift, if any population is present in higher- n states. For hydrogen atoms created by charge exchange, as in Ref. [17] and our ongoing measurement, the 3S state has the largest charge-exchange cross section for states with $n>2$. For a 50-keV proton beam, the ratio of the charge-exchange cross sections [26] for the $3S_{1/2}$ and $2S_{1/2}$ states is approximately 0.34.

To illustrate the effect of the previous sections with a more concrete example, we calculate the shift that would be caused in the SOF measurement of the $2S_{1/2}$ -to- $2P_{1/2}$ Lamb-shift interval of Ref. [17], if the experiment starts with a relative 3S-to-2S population ratio of 0.34. We emphasize that the population in the 3S state could be different for the actual measurement of Ref. [17] (for example, due to multiple collisions during charge exchange), and also that other high- n states could shift the measured resonance. The calculation here, however, sets a scale for possible shifts.

The calculation performed includes all states for $n=1, 2$, and 3. These include all hyperfine states (all values of quantum number f) and all sublevels (all values of m_f), for a total of 56 states. Thus, Eq. (1) must be expanded to $56^2=3136$ equations. These equations have been numerically integrated through a trajectory that takes 400 ns to traverse. The fields along this trajectory are those identified as configuration 1 in Ref. [27]. As suggested in that reference, a trajectory that is 1.265 mm from the axis is used (as this distance is the root-mean-squared distance from the axis for the extended beam of atoms in that work). The off-axis trajectory leads to two components of the electric field, with the largest component driving $\Delta m_f=0$ transitions and the smaller component driving $\Delta m_f=\pm 1$ transitions. The fields do not turn on and off suddenly, as was assumed in Section III, but rather follow the more realistic profiles described in Ref. [27].

The 400-ns trajectory includes a 35-ns-long preparation field at 1110 MHz (which depletes the 2S $f=1$ population), two 10-ns-long fields to perform the SOF measurement of the $2S_{1/2}(f=0)$ -to- $2P_{1/2}(f=1)$ transition (with the centers of these fields separated by 15 ns), and a 10-ns-long field at 910 MHz used to quench the remaining 2S population by mixing the 2S state with the quickly-decaying 2P state. As in Ref. [27], the amplitudes used for these fields are 26, 11.4, and 11 V/cm, respectively. As in the experiment, the $n=2$ -to- $n=1$ radiative decay (Lyman- α fluorescence) is monitored during the quench field. The calculation is repeated for different phases of each of these fields, and averaged over these phases, as well as taking the difference between the in-phase and 180-degree-out-of-phase signals for the SOF

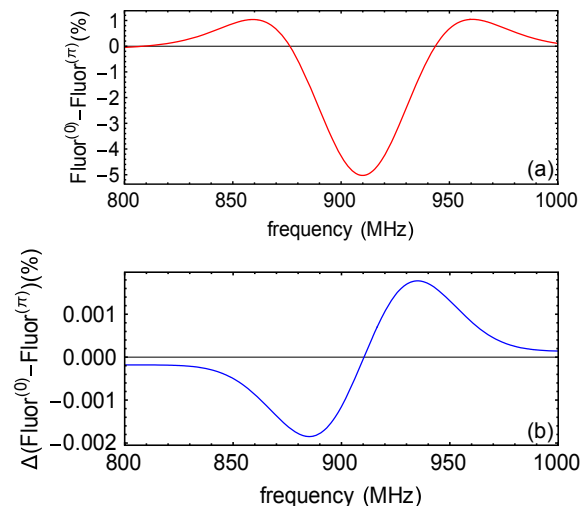


FIG. 4. (Color online) Line shapes for an SOF $2S_{1/2}$ -to- $2P_{1/2}$ atomic hydrogen Lamb-shift measurement. The full line shape for the Lyman- α fluorescence predicted for an initial population of 1.0 divided equally among the four $2S_{1/2}$ states and a population of 0.34 divided equally among the four $3S_{1/2}$ states is shown in (a). This line shape includes a small distortion due to the fact that coherences between 3S and 3P states can radiatively decay into coherences between 2S and 2P states. The difference between the calculations with and without this decay of coherences for the SOF measurement are shown in (b). The dispersion in (b) is due to the same effect as that shown in Fig. 3(c). The distortion in (b) causes a shift of approximately -9.5 kHz.

fields. The signals (based on Lyman- α fluorescence induced by the quench fields) are calculated for a range of frequencies for the SOF fields.

The calculation is computationally intensive and employed the SHARCNET computer cluster. This calculation is far beyond that which could have been performed at the time of the measurement of Ref. [17]. The SOF lineshape obtained from integrating the equations is shown in Fig. 4(a). Part (b) of the figure shows the difference between the calculation of the SOF line shape with and without the terms analogous to the square-root term in Eq. (1c), that is, with and without allowing coherences in the $n=3$ states to radiatively decay to coherences in the $n=2$ states. The difference reveals a dispersion line shape, similar to that of Fig. 3(c). This dispersion curve results from the sum of all of the interferences between 2S-to-2P and 3S-to-3P resonances, with the sign of each interference determined by the relative signs of the matrix elements of the 3S-to-2P and 3P-to-2S decay paths. The shift caused by the presence of 3S atoms is dominated by the dispersion line shape due to radiative decay of coherences between 3S states and 3P states (which decay into coherences between 2S and 2P states). Using the set of frequencies of Ref. [27], and using the symmetric-points method described in that work, the calculated shift due to the 3S atoms is -9.5 kHz. A +9.5 kHz correction would have to be applied to the measurement

of Ref. [17] to compensate for this shift if only the 3S state were present, and if its population relative to the 2S state were 0.34. However, to calculate the full shift, a similar analysis would also have to be performed for higher- n states, and precise knowledge of the populations in each of the $n > 2$ states would be necessary. It is not possible to infer these populations to a sufficient level of accuracy from Refs. [17] and [27]. The calculation presented here does, however, conclude that the correction can be expected to be on the 10-kHz scale.

The calculation presented in this section is far more complicated than the simple four-level model of Section III, but the physics dominating the calculated shifts remains the same. The parameters used for Figs. 2 and 3 correspond to the four-level system consisting of $|2S_{1/2}, f=0, m_f=0\rangle$, $|2P_{1/2}, f=1, m_f=0\rangle$, $|3S_{1/2}, f=0, m_f=0\rangle$, and $|3P_{3/2}, f=1, m_f=0\rangle$. The full calculation extends this four-level model to include all of the states for $n=1, 2$ and 3 , which allows for more decay channels, for more coherences, and for more interfering resonances.

The 10-kHz scale of this interference shift makes it important, since the SOF measurement of Ref. [17] has a precision of 9 kHz, and the discrepancy between this measurement and the interval calculated [28] using the new, more accurate measurement of the proton charge radius from muonic hydrogen [19, 20] is 13 kHz. The ongoing

Lamb-shift measurement by our group has a precision goal of a few kHz, and, therefore, these shifts will have to be considered very carefully.

V. SUMMARY

We have identified a new systematic effect important to precision measurements. The effect allows for an interference between two resonant transitions that do not have a common initial nor final state, but, rather, have states connected by radiative decay. The interference causes a line-shape distortion and a shift for the precision measurement. We find that this effect is large enough to have an important impact on the existing [17] and ongoing measurements of the hydrogen $n=2$ Lamb shift. As such, they may contribute to the current discrepancy [21–23] between muonic and electronic measurements of the proton radius.

VI. ACKNOWLEDGEMENTS

This work is supported by NSERC and CRC and used SHARCNET for computation.

-
- [1] M. Horbatsch and E. A. Hessels, Phys. Rev. A **82**, 052519 (2010).
 - [2] M. Horbatsch and E. A. Hessels, Phys. Rev. A **84**, 032508 (2011).
 - [3] A. Marsman, M. Horbatsch, and E. A. Hessels, Phys. Rev. A **86**, 012510 (2012).
 - [4] A. Marsman, M. Horbatsch, and E. A. Hessels, Phys. Rev. A **86**, 040501 (2012).
 - [5] A. Marsman, E. A. Hessels, and M. Horbatsch, Phys. Rev. A **89**, 043403 (2014).
 - [6] A. Marsman, M. Horbatsch, and E. A. Hessels, Phys. Rev. A **91**, 062506 (2015).
 - [7] C. J. Sansonetti, C. E. Simien, J. D. Gillaspay, J. N. Tan, S. M. Brewer, R. C. Brown, S. Wu, and J. V. Porto, Phys. Rev. Lett. **107**, 023001 (2011).
 - [8] R. C. Brown, S. J. Wu, J. V. Porto, C. J. Sansonetti, C. E. Simien, S. M. Brewer, J. N. Tan, and J. D. Gillaspay, Phys. Rev. A **87**, 032504 (2013).
 - [9] C. J. Sansonetti, C. E. Simien, J. D. Gillaspay, J. N. Tan, S. M. Brewer, R. C. Brown, S. J. Wu, and J. V. Porto, Phys. Rev. Lett. **109**, 259901 (2012).
 - [10] P. Amaro, B. Franke, J. J. Krauth, M. Diepold, F. Fratini, L. Safari, J. Machado, A. Antognini, F. Kottmann, P. Indelicato, R. Pohl, and J. P. Santos, Phys. Rev. A **92**, 022514 (2015).
 - [11] D. C. Yost, A. Matveev, E. Peters, A. Beyer, T. W. Hänsch, and T. Udem, Phys. Rev. A **90**, 012512 (2014).
 - [12] P. Amaro, F. Fratini, L. Safari, A. Antognini, P. Indelicato, R. Pohl, and J. P. Santos, Phys. Rev. A **92**, 062506 (2015).
 - [13] A. A. Buchheit and G. Morigi, Phys. Rev. A **94**, 042111 (2016).
 - [14] H. Fleurbaey, F. Biraben, L. Julien, J.-P. Karr, and F. Nez, Phys. Rev. A **95**, 052503 (2017).
 - [15] G.-P. Feng, X. Zheng, Y. R. Sun, and S.-M. Hu, Phys. Rev. A **91**, 030502 (2015).
 - [16] G.-W. Truong, J. D. Anstie, E. F. May, T. M. Stace, and A. N. Luiten, **6** (2015).
 - [17] S. R. Lundeen and F. M. Pipkin, Phys. Rev. Lett. **46**, 232 (1981).
 - [18] For an overview of measurements of the hydrogen Lamb shifts and theoretical predictions, see Refs. [28] and [29].
 - [19] R. Pohl, A. Antognini, F. Nez, F. D. Amaro, F. Biraben, J. M. Cardoso, D. S. Covita, A. Dax, S. Dhawan, L. M. Fernandes, *et al.*, Nature **466**, 213 (2010).
 - [20] A. Antognini, F. Nez, K. Schuhmann, F. D. Amaro, F. Biraben, J. M. Cardoso, D. S. Covita, A. Dax, S. Dhawan, M. Diepold, *et al.*, Science **339**, 417 (2013).
 - [21] J. C. Bernauer and R. Pohl, Scientific American **310**, 32 (2014).
 - [22] R. Pohl, R. Gilman, G. A. Miller, and K. Pachucki, Annual Review of Nuclear and Particle Science **63**, 175 (2013).
 - [23] C. E. Carlson, Progress in Particle and Nuclear Physics **82**, 59 (2015).
 - [24] D. A. Cardimona and C. R. Stroud, Phys. Rev. A **27**, 2456 (1983).
 - [25] N. F. Ramsey, Phys. Rev. **76**, 996 (1949).
 - [26] R. H. Hughes, C. A. Stigers, B. M. Doughty, and E. D. Stokes, Phys. Rev. A **1**, 1424 (1970).
 - [27] S. R. Lundeen and F. M. Pipkin, Metrologia **22**, 9 (1986).

- [28] M. Horbatsch and E. Hessels, Physical Review A **93**, 022513 (2016).
- [29] P. J. Mohr, D. B. Newell, and B. N. Taylor, Journal of Physical and Chemical Reference Data **45**, 043102